Deviation of continuum formulation for solid-solid momentum transfer rate in terms of spatial averaging in mixtures with large particle size ratios

Shah Srujal, Jalali Payman

DOI: 10.1016/j.powtec.2020.01.011

Deviation of continuum formulation for solid-solid momentum transfer rate in terms of spatial averaging in mixtures with large particle size ratios

Srujal Shah*, Payman Jalali
School of Energy Systems, Lappeenranta-Lahti University of Technology LUT, P.O. Box 20, FI-53851 Lappeenranta, Finland
***Corresponding Author**: E-mail: srujal.shah@lut.fi (S. Shah), payman.jalali@lut.fi (P. Jalali)

Abstract

In a fluidized bed system, mean trajectories of fuel particles within the bed of fluidized inert particles are governed by the associated drag forces and characterize hydrodynamic, chemical and thermal processes taken place in the system. A large particle size ratio between the bed material and the fuel particles affects the hydrodynamics of gas-solid multiphase flows via influencing the drag forces between solid phases. The present work focuses on the analysis of forces between the two solid phases with large size ratios using the Lagrangian simulations of discrete element method (DEM). The results are spatially averaged over variable control volume size for comparison to the continuum interphase momentum transfer model. Using our DEM simulation results, a correction factor of drag force is presented versus the size of averaging control volume usable in continuum models. In addition, the role of inhomogeneity of particles distribution within the averaging box is discussed.

Keywords

Discrete element method; Solid-solid drag; Continuum model; Simulations; Spatial averaging; Correction factor

1. Introduction

Due to its principal advantage in the utilization of various types of fuels, the circulating fluidized bed technology has proven to be an efficient way for combustion in heat and power generation [1]. Computer simulations are often used for better understanding of the gas-solid flows in circulating fluidized beds. In the simulations, the modeling of particles phase is based on either the Eulerian formulation [2] or the Lagrangian methods such as the discrete element method (DEM) [3]. Regardless of advances in computational power to perform DEM simulations [4], its application is still limited to the simulation of small scale systems. Thus, the Eulerian approach is practically preferred and often used in simulations of fluidized beds.

In the fluidized bed combustion process, the bed material typically consists of sand, ash particles, and fuel particles which are usually coal or biomass particles. Due to the presence of different particle types (such as the inert bed particles and the fuel particles), the interphase momentum transfer or the drag force between the solid phases is also significant in addition to the gas-solid drag force. Various attempts have been made for formulating the solid-solid drag force which has resulted in several correlations in the literature [5]. All these formulations are based on the kinetic theory of granular flows. These correlations may include the granular temperature or not. Among the presented correlations, the model formulated by Syamlal [6] is highly used in Eulerian simulations. A basic assumption of this model is associated with the homogeneity of particles distribution. Moreover, if the size ratio of particles is large, then a local inhomogeneity is predicted due to the presence of large particles [7].

The Eulerian approach for simulations of gas-solid flows in fluidized beds requires fine grids to obtain reliable flow profiles such as the solids concentration and the mass flow rate [8]. Simulations using fine grids (in the order of few particle diameters) are not practical for large scale units; instead, coarse grids are created. The use of coarse grids results in the volumetric over-averaging of drag force between the phases. Thus, there is a need to formulate

sub-grid models for the gas-solid and the solid-solid drag forces, which can be used in coarse grid simulations. For the case of monodisperse systems, there are numerous studies dealing with the formulation of sub-grid models. A commonly used approach is the filtered or spatial averaging approach [9–14]. In this type of approach, the results from the fine grid simulations are filtered over different averaging sizes to formulate sub-grid models that can be used in coarse grid simulations. However, for the case of bidisperse systems, the topic is relatively new and only few efforts have been presented in the literature [15,16].

Indeed, the filter size (averaging control volume size) is a dominant parameter, but additional markers have been investigated for sub-grid drag modeling of gas-solid flows. In the earlier works for monodisperse systems [9,17,18], one-marker model was presented as the function of solid volume fraction. Later, the effect of gas-solid slip velocity was also taken into account [19,20] as an additional marker. In addition, the variable granular temperature as represented by particle velocity fluctuation [21], and the sub-grid model considering the effects of local inhomogeneity within a grid [22] were taken into account. Recently, the effects of material properties on the sub-grid drag model have been investigated [23]. Thus several parameters have been studied in formulating sub-grid models for predicting correct hydrodynamics of gas-solid flows. The above markers should be taken into account for developing sub-grid models for bidisperse systems, which will be focused in our future works.

In the current study, the solid-solid momentum transfer rate between spherical particles with large size ratios is computed from the contact forces between the particles of different sizes obtained from DEM. The forces are averaged over different volume sizes and compared to the volumetric momentum transfer rate model used in the Eulerian simulations. The key question is how accurate the continuum model can represent the volumetric momentum transfer rate as a function of the size of the averaging region within which inhomogeneity created due to a large size ratio. Therefore, one may introduce a correction factor to the existing continuum

models of the solid-solid momentum transfer rate in order to extend their applicability to the coarse grid Eulerian simulations. The forces obtained from both the DEM and the continuum formulation are presented and compared for various averaging sizes. Simulations are also performed to study the inhomogeneous conditions in which particles are not uniformly distributed within the control volume.

2. Modeling methodology

2.1. Geometry

There is no confining boundaries, but the distribution of particles are given within a domain with a rectangular cross-section. A stream of small particles passes over a big particle. The cross-section of the stream of small particles is $0.02 \times 0.02\ m^2$ with the height of $0.06\ m$. The position of the big particle is at the center of the stream during the simulation. Figure 1 demonstrates the initial configuration of the stream of small particles and the big particle at the center of the stream cross-section.

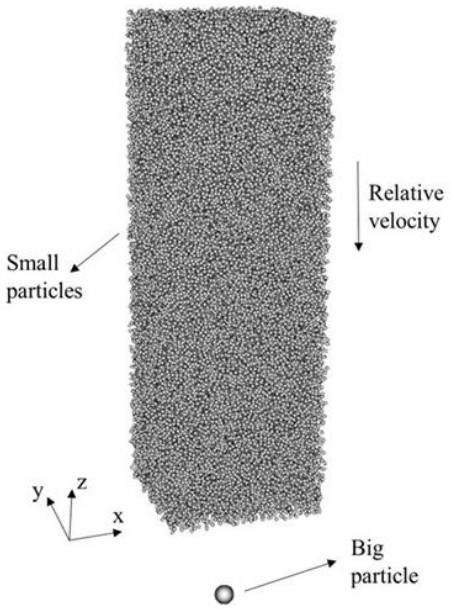

Fig. 1. Initial arrangement of small particles and big particle.

2.2. Computational method

In this work, an open source software, LIGGGHTS®, is used which is based on the DEM for the Lagrangian simulations of the solid phases [24]. The DEM resolves the kinematics of individual particles using the Newton's second law from the instantaneous normal and tangential forces due to the contacts with neighboring particles. Individual particles can have translational and rotational motions. Applying the Newton's law for a particle i with mass m_i, the moment of inertia I_i, translational velocity $\boldsymbol{v}_i$ and angular velocity $\boldsymbol{\omega}_i$, the equations of motion can be written as following

$$m_i \frac{d\boldsymbol{v}_i}{dt} = \sum_j \left(\boldsymbol{F}_{n,ij} + \boldsymbol{F}_{t,ij}\right), \quad (1)$$

$$I_i \frac{d\boldsymbol{\omega}_i}{dt} = \sum_j \boldsymbol{T}_{ij}, \quad (2)$$

where $\boldsymbol{F}_{n,ij}$ and $\boldsymbol{F}_{t,ij}$ are the normal and tangential components of the contact forces between particles j and i. The effect of gravity is not included in this study and there is no fluid phase considered. $\boldsymbol{T}_{ij}$ is the torque imposed by the tangential component of the contact force from particle i on particle j. The contact forces in the normal and tangential directions are determined by the linear spring-dashpot model. The contact forces constituting of two terms corresponding to the stiffness and the damping coefficients can be computed from the modified Hertz-Mindlin model [25,26] as follows

$$\boldsymbol{F}_{n,ij} = -\frac{4}{3} Y^* \sqrt{R^*} \delta_n^{3/2} \boldsymbol{n}_{ij} + 2\sqrt{\frac{5}{6}} \beta \sqrt{S_n m^*} \boldsymbol{v}_{n,ij}, \quad (3)$$

$$\boldsymbol{F}_{t,ij} = -8G^* \sqrt{R^* \delta_n} \boldsymbol{\delta}_{t,ij} + 2\sqrt{\frac{5}{6}} \beta \sqrt{S_t m^*} \boldsymbol{v}_{t,ij}, \quad (4)$$

where $S_n = 2Y^* \sqrt{R^* \delta_n}$ and $S_t = 8G^* \sqrt{R^* \delta_n}$. Here, δ_n is the normal overlap distance between the particles, $\boldsymbol{n}_{ij}$ is the normal unit vector directed from the center of particle i to that of particle j, $\boldsymbol{\delta}_{t,ij}$ is the tangential displacement vector calculated by integrating the relative tangential velocity at the contact over time, $\boldsymbol{v}_{n,ij}$ and $\boldsymbol{v}_{t,ij}$ are the normal and tangential

components of the relative velocity of particles i and j. The expression for the torque is given as $\boldsymbol{T}_{ij} = R_i \boldsymbol{n}_{ij} \times \boldsymbol{F}_{t,ij}$. The magnitude of the tangential force is truncated by the Coulomb friction criterion: $\boldsymbol{F}_{t,ij} \leq \mu_f \boldsymbol{F}_{n,ij}$, where μ_f is the friction coefficient. In the above Eqs. (3) and (4), the term β is expressed as a function of restitution coefficient e given by

$$\beta = \frac{ln(e)}{\sqrt{ln^2(e)+\pi^2}}. \tag{5}$$

The other symbols mentioned in Eqs. (3) and (4), are given as,

$$\frac{1}{Y^*} = \frac{1-\nu_i^2}{Y_i} + \frac{1-\nu_j^2}{Y_j}, \tag{6}$$

$$\frac{1}{R^*} = \frac{1}{R_i} + \frac{1}{R_j}, \tag{7}$$

$$\frac{1}{m^*} = \frac{1}{m_i} + \frac{1}{m_j}, \tag{8}$$

$$\frac{1}{G^*} = \frac{2(2-\nu_i)(1+\nu_i)}{Y_i} + \frac{2(2-\nu_j)(1+\nu_j)}{Y_j}, \tag{9}$$

where Y^* is the effective Young's modulus, G^* is the effective shear modulus, ν is the Poisson's ratio, R^* is the effective radius and m^* is the effective mass.

In order to compare the DEM results with the continuum formula, Syamlal's formula is used for the volumetric solid-solid momentum transfer rate. The momentum transfer rate between the two solid phases corresponding to big (b) and small (s) particles is given by the following expression [6,7],

$$\boldsymbol{F}_{sb} = \frac{3(1+e)\left(\pi/2+\mu_f \pi^2/8\right)\alpha_s \alpha_b \rho_s \rho_b (d_s+d_b)^2 g_0 |\boldsymbol{u}_b - \boldsymbol{u}_s|}{2\pi(\rho_s d_s^3 + \rho_b d_b^3)} (\boldsymbol{u}_b - \boldsymbol{u}_s), \tag{10}$$

where the radial distribution function at contact is $g_0 = \frac{1}{\alpha_g} + \frac{3 d_s d_b}{\alpha_g^2 (d_s+d_b)} \left(\frac{\alpha_s}{d_s} + \frac{\alpha_b}{d_b}\right)$. Here, α_g is the void fraction as $1 - \alpha_b - \alpha_s$. In addition to the volume fractions, the volumetric momentum transfer rate between phase s and phase b contains the diameter and density of particles, collisional properties including the restitution and friction coefficients, and the averaged velocities of both phases.

2.3. Simulations details

In the simulated cases shown in Fig. 1, a big particle is fixed in space. Three different cases are analyzed in which the diameter of the big particle is considered with the size ratios of $5, 10$ and 15 with respect to the size of small particles. A stream of small particles is set to pass over the big particle with its lateral position at the center of the stream cross-section. The initial velocity of the small particles is $0.5\ {}^{m}/_{s}$ in the negative z-direction. The simulation parameters are given in Table 1. The mechanical properties of the material considered in Table 1 are similar to the glass beads which are mainly found in the literature for performing small scale simulations.

Table 1. Parameter values used in simulations.

Parameter	Value
Small particle diameter, d_s	$0.0005\ m$
Big particle diameter, d_b	$0.0025\ m, 0.005\ m, 0.0075\ m$
Particle density: ρ_s, ρ_b	$2500\ {}^{kg}/_{m^3}$
Young's modulus: Y_s, Y_b	$10^9\ {}^{kg}/_{ms^2}$
Poisson's ratio: ν_s, ν_b	0.2
Friction coefficient: μ_{s-b}, μ_{s-s}	0.15
Restitution coefficient: e_{s-b}, e_{s-s}	0.95
Simulation time	$0.2\ s$
Time step size	2.5×10^{-7} s

3. Results and discussion

3.1. Forces from DEM

For all the cases of the big particle diameters, a stream of small particles is allowed to pass over it. Figure 2 shows the snapshots of the stream of small particles passing over the fixed big particle with an initial uniform velocity. The snapshots are presented for the case with

$d_b = 15d_s$. The snapshots shown in Fig. 2 are presented only for the small particles located in the back half of the stream, and the front half of the stream is omitted for the sake of clear visualization. It can be seen that during the transient time, the stream of small particles approaches the big particle, results in collisions and then gradually pass over the big particle. As the stream particles collide with the big particle, there is some decrease in the relative velocity, however, the velocity of stream particles away from the big particle does not alter much.

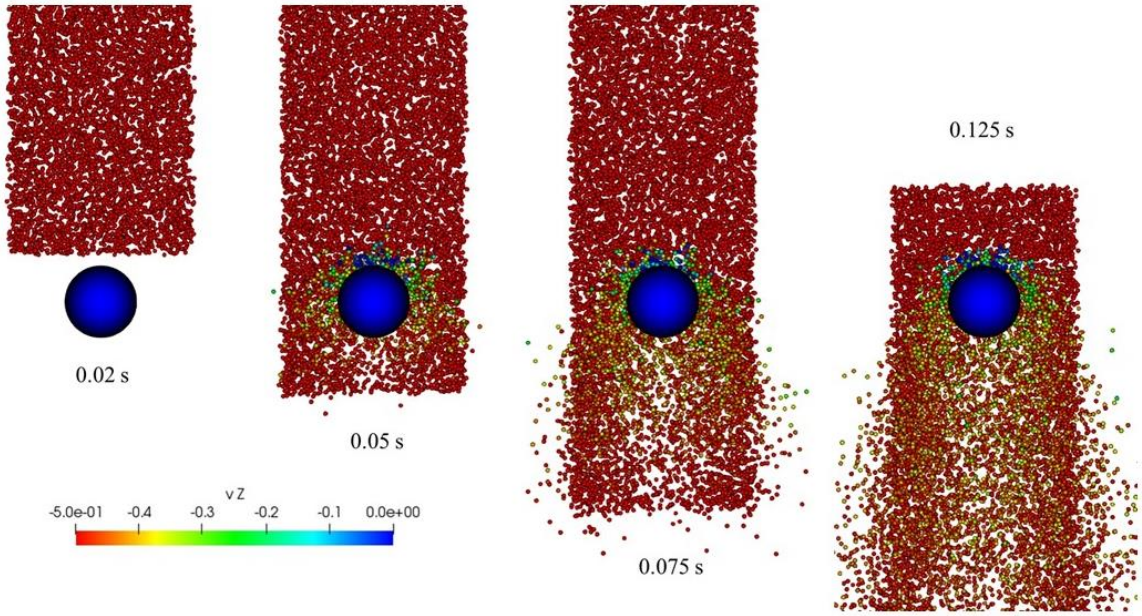

Fig. 2. Snapshots of small particles passing over the fixed big particle colored by their velocities. Note that only the small particles located in the half-part of the stream are shown for better visualization.

As mentioned earlier, the effect of gravity is not included to avoid the acceleration of the stream. The interphase forces between particles from DEM include the normal and tangential components of the contact forces as given in Eq. (1). Since the direction of the relative velocity between the stream particles and the big particle is in the vertical direction, the instantaneous force in z-direction exerted on the big particle are demonstrated in Fig. 3a. It can be seen from Fig. 3a that the instantaneous force is highly fluctuating which originates

from individual collisions with the small particles of the stream. In the studied solid volume fractions standing for dilute regimes, collisions are majorly isolated events with quiescent times between successive collisions. The mean effective force acts within a time window sufficiently larger than the duration of single collisions. Note that the fluctuations start with the collisions and end when the particles completely pass over the big particle.

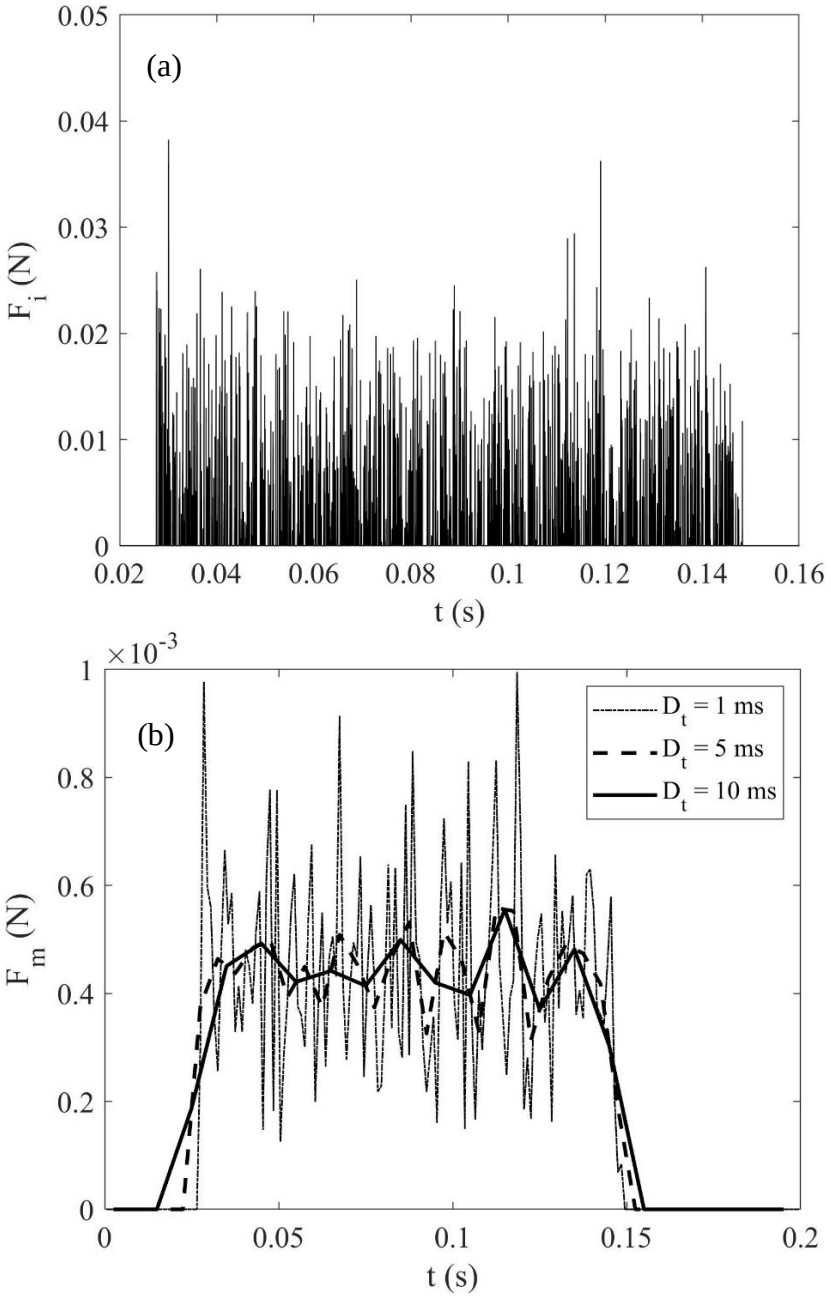

Fig. 3. (a) Instantaneous force in the vertical direction (z-direction) versus time calculated from the DEM for the case of big particle diameter as 0.0025 m. (b) The time-averaged force exerted on the big particle versus time using different sampling times (D_t) as 1 ms, 5 ms and 10 ms.

As mentioned above, the averaging time window must contain sufficient number of collisions to obtain statistically correct average values. For example, the sampling time of $D_t = 1\,ms$ corresponds to $4000d_t$, where d_t is the time step size used in the simulations. The variation of mean forces with time obtained from averaging the instantaneous forces using different averaging time windows are presented in Fig. 3b. Previously, similar analysis was presented for the mean forces versus averaging time window [27]. By increasing the size of the averaging time, the fluctuations of the mean forces with time are damped out. The concept of averaging over a time window resembles the measurement of force by a strain gauge which senses a collective effect of isolated collisions through the sampling period of the sensor. Note that, the mean forces are significantly smaller than the magnitudes of the spikes of instantaneous forces, which is a result of time averaging over the major portion of time being as the quiescent times between successive collisions. It is also noted from Fig. 3b that the fluctuations start to damp out when higher averaging time window of $5\,ms$ is used, while the mean forces are highly fluctuating with $1\,ms$. In this work, the averaging time window is chosen as $2.5\,ms$.

3.2. Continuum model prediction versus DEM

The main aim of this work is to analyze the effect of spatial averaging on the continuum model for solid-solid momentum transfer rate used in Eulerian models. The computational methods developed to solve Eulerian equations discretize the domain into a finite number of control volumes. For the Eulerian simulations of monodisperse particle systems, the grid sizes of the order of few particle diameters have been suggested in literature to yield realistic flow profiles. For instance, the grid sizes are shown to be in the order of 10 particle diameters for the case of risers [28] and in the order of 3 particle diameters for the case of bubbling fluidized beds [29]. For the case of bidisperse systems, there is no reported study introducing suitable

grid resolution. In the development of filtered models for bidisperse gas-particle flow systems [16], the minimum grid resolution was about 5 times the sum of particle diameters at the size ratio of 4. They studied fine particles from the group of Geldart A particles. In this study, the small particles were considered much coarser which typically represent the inert bed material whereas the big particles stand for the biomass particles commonly used in circulating fluidized beds. If the size ratio between interacting particles gets larger, e.g. in the order of 10 or higher, the grid size (the control volume here) may be taken in the same order of the big particle diameter because it collects a significant number of contacts and collisions from many neighboring small particles.

For particles in bidisperse mixtures of diameters d_s and d_b, an appropriate value for the size of the control volume could be taken as $(d_s + d_b)$. The solid structures in gas–solid multiphase flows consist of meso-scale structures such as clusters and streamers of particles. The sizes of these structures vary over length scales from few millimeters to few centimeters, therefore, fine grids must be used to resolve such flow structures. In addition to monodisperse systems, these flow structures have been studied for bidisperse systems using the Eulerian approach [15] in which the appropriate size of the averaging control volume was not necessarily the minimum grid size to resolve meso-scale flow structures in the Eulerian simulations of bidisperse systems. Here, we have used the control volume size of $(d_s + d_b)$ as the minimum scale resolution, and then perform spatial averaging over coarser scales to demonstrate the need for sub-grid modeling of solid-solid momentum transfer rate by means of DEM.

The mean volumetric momentum transfer rate between the big and small particles can be calculated by averaging the instantaneous force calculated directly from the DEM as given by the following formula [7],

$$\langle \boldsymbol{F}_m \rangle = \frac{\sum_{j=1}^{N_t} \sum_{i=1}^{N_{bs}} \boldsymbol{F}_{ij}}{V N_{bs} N_t}, \tag{11}$$

where N_{bs} refers to the number of contacts between the big and the small particles at any time step j during the averaging time window D_t. The time interval refers to the sampling time as $N_t \cdot d_t$, where d_t is the time step size for simulations. Also, N_t refers to the number of time steps fit in D_t. In this study, the averaging time window is taken as $2.5\ ms$ corresponding to the value of N_t as 10^4. If the big particle contacts several small particles simultaneously, the vertical force (direction of relative velocity) is calculated as the net value of the projection of the normal and tangential components onto the vertical axis. The mean force is then calculated over the control volume V around the big particle.

The volumetric momentum transfer rate from DEM is compared to that predicted by the continuum formula by Syamlal (Eq. 10). For this purpose, all information of particles in time have been used to calculate the volume fractions and phase velocities inside the control volume. Figure 4 shows the volumetric momentum transfer rate between the big and small particles calculated from both the DEM and Syamlal's formula for three diameters of the big particle. In Figs. 4a-c, the size of the control volume is the sum of the particle diameters, i.e. $(d_s + d_b)$. Figures 4a, 4b and 4c correspond to the cases with the size of the big particle as $5d_s$, $10d_s$ and $15d_s$, respectively.

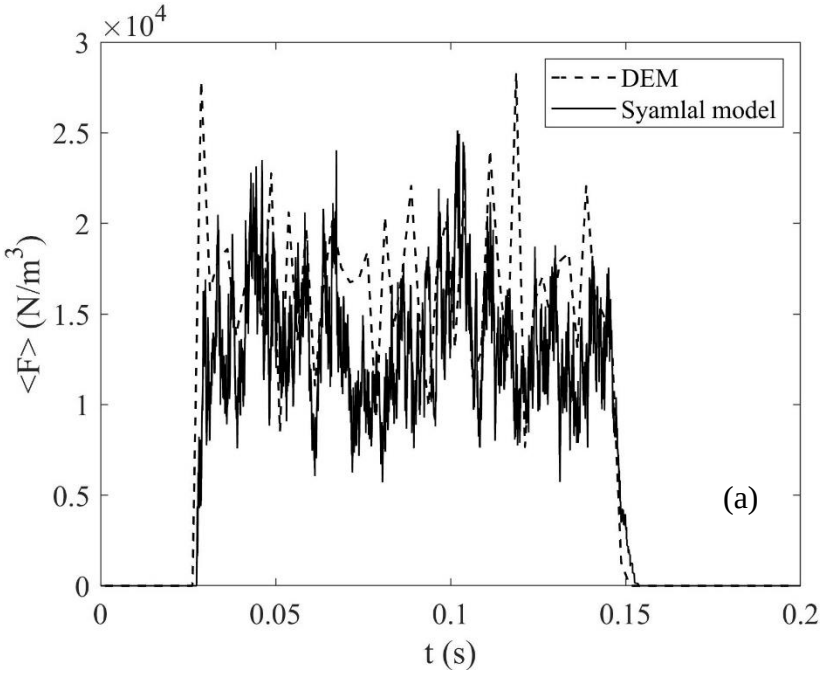

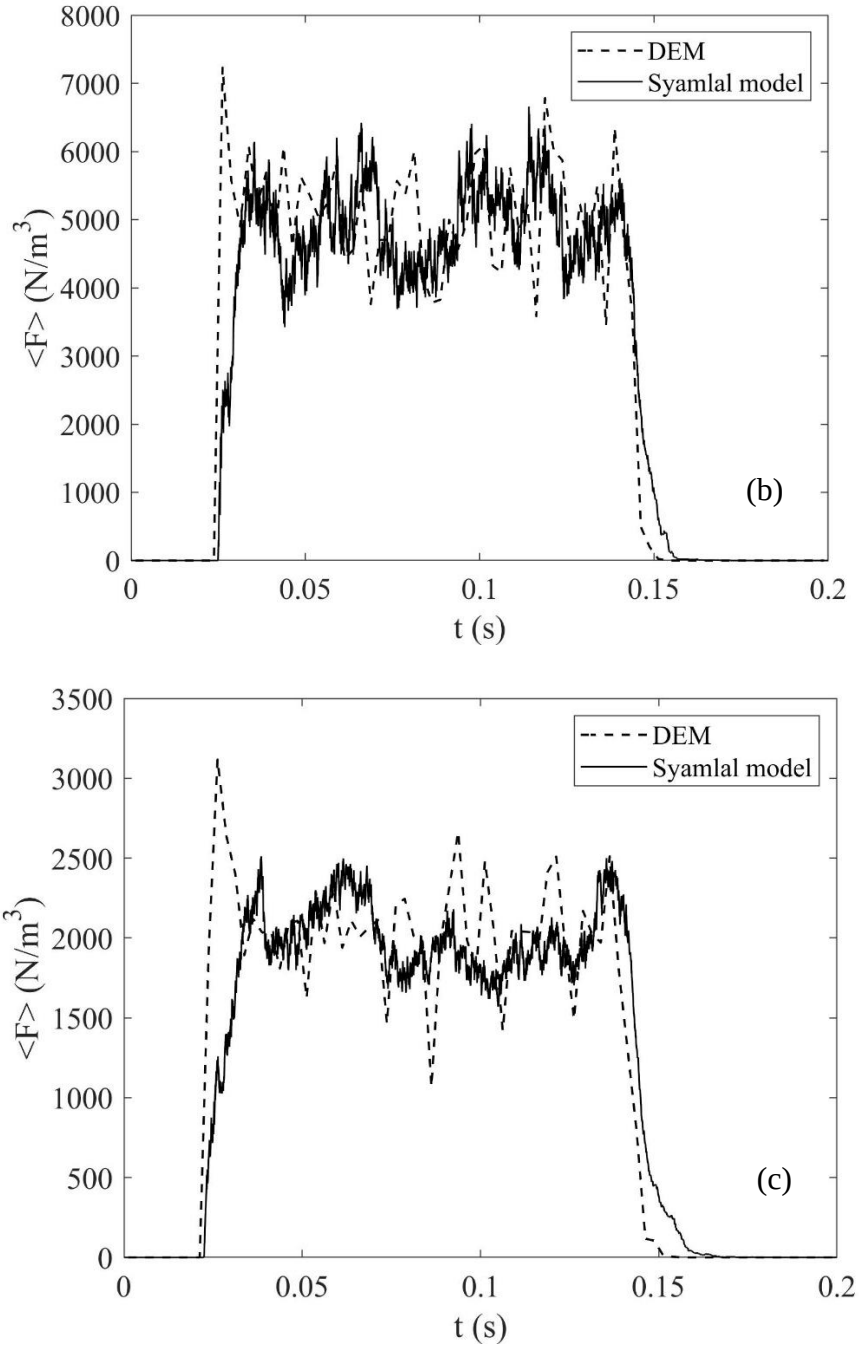

Fig. 4. Comparison of momentum transfer rate between the big and small particles calculated using DEM and Syamlal's model for big particle diameter as (a) $5d_s$, (b) $10d_s$ and (c) $15d_s$.

It should be noted that the small particles volume fraction in the stream is not the same for different big particle diameters. The small particles volume fraction in the stream was chosen as 0.16, 0.1 and 0.06, corresponding to the simulation cases with the diameter of big particle as $5d_s$, $10d_s$ and $15d_s$, respectively. The reason for using different volume fractions

in the stream for all three cases of big particle diameters was to get similar trend of the momentum transfer rate between the DEM and the Syamlal's model when using the control volume size as $(d_s + d_b)$. As Fig. 4 demonstrates, the time variation of mean forces on the big particle obtained from DEM and the continuum model (based on the solid volume fraction and velocity data from DEM) are similar. Minor temporal discrepancy between the results of the DEM and continuum model could be a result of averaging and existing simplifying assumptions in the derivation of Syamlal's formula. We have performed a spatial averaging associated with the Syamlal's prediction to introduce correction factors needed in coarse grid simulations, as presented in the next section.

3.3. Correction factor to Syamlal's model

We study the effect of spatial averaging around the big particle on the momentum transfer rate between the big and small particles. Different averaging regions are selected around the big particle such that the center of the big particle and the averaging regions are aligned. Following various spatial averaging within different sizes of averaging control volume, an expression can be developed to formulate the correction for the continuum model. Mathematically, the expression can be simply written as,

$$\langle \boldsymbol{F}_{DEM} \rangle = \omega \langle \boldsymbol{F}_{Sy} \rangle, \qquad (12)$$

where, <> is the spatial averaging operator and ω is the correction factor which needs to be determined. The spatial averaging operator is applied to obtain the volumetric momentum transfer rate between two solid phases calculated from the DEM and the Syamlal's formula.

As seen from Figs. 4a-c, the momentum transfer rate increases during the initial moments of encounter and it decays at the end. This is the time span during which the stream enters and leaves the averaging control volume. Excluding the beginning and the end of the encounter, the flow exhibits fluctuating but uniform mean rate of momentum transfer. The

volume fraction of small particles remains uniform during the encounter period. As seen earlier in Fig. 3b, the fluctuations can be reduced by increasing the averaging time window. The variation of the correction factor for different averaging sizes in various size ratios studied in this work is presented in Figs. 5a-c. Interestingly, the correction factor during the transient period at the start of encounter reaches as high as 3 to 3.5, which is about 4 times higher than the steady value. This indicates that the correction factor can be highly dependent of the transient conditions which requires an extensive study on the issue. However, this study only concerns the steady or quasi-steady conditions. It can be seen from Figs. 5a-c that during the steady period of the encounter, the correction factor decreases asymptotically when the size of the averaging region increases.

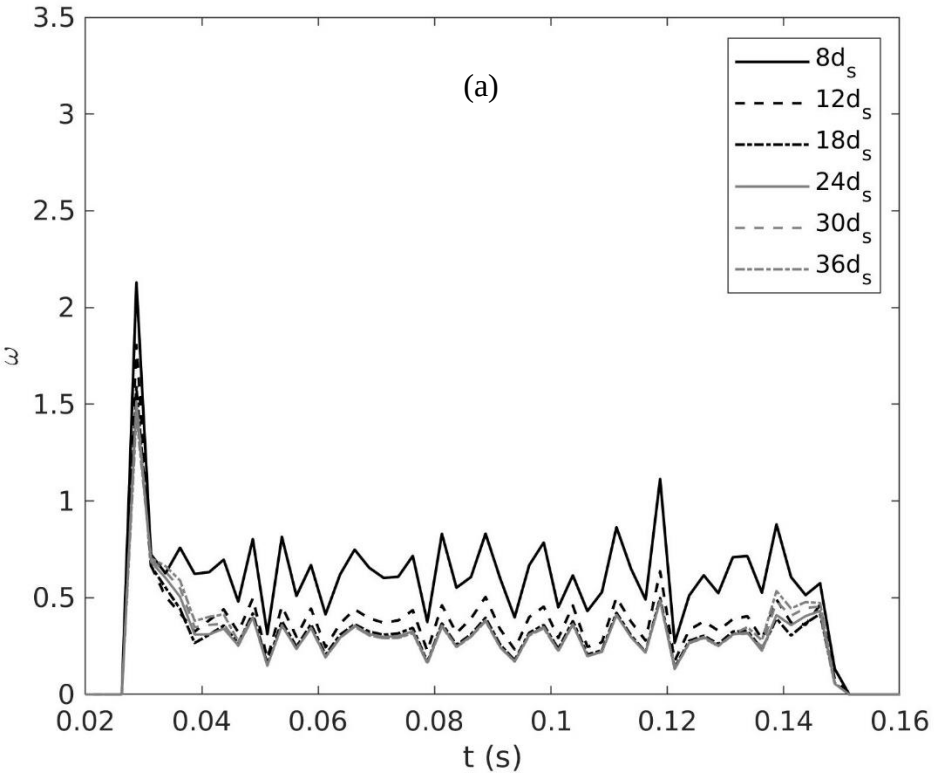

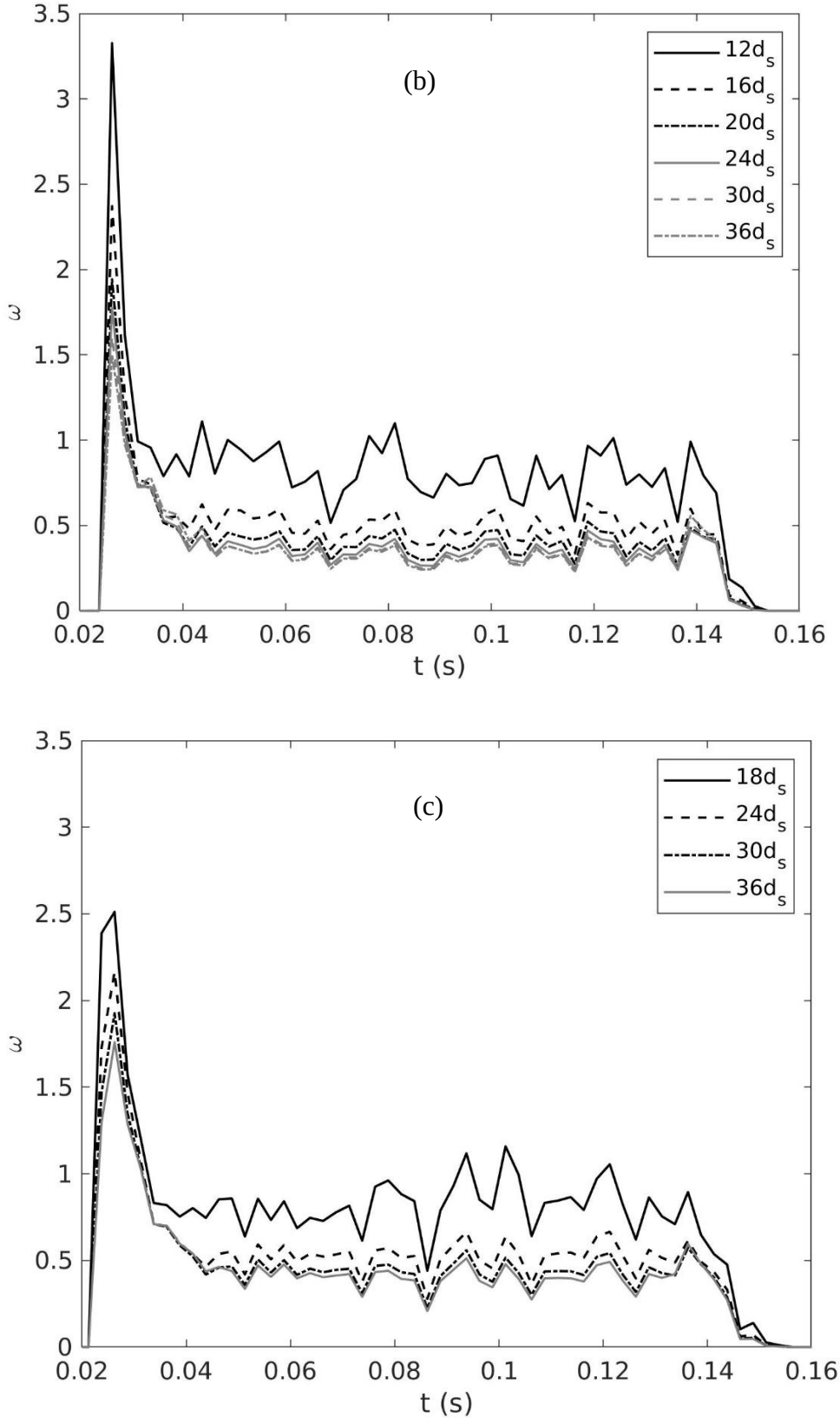

Fig. 5. Comparison of correction factor for various averaging region sizes for the big particle diameter as (a) $5d_s$, (b) $10d_s$ and (c) $15d_s$.

In order to reveal the behavior of the correction factor with the size of averaging control volume, we demonstrate its mean value obtained during the steady period of each simulation versus the averaging size in Fig. 6. It reveals that for all size ratios, the correction factor decreases with the size of the averaging control volume. This trend is in accordance to filtered drag models in monodisperse [9] and bidisperse systems [16]. Moreover, for all size ratios, the correction factor is close to 1 when using the averaging size of $(d_s + d_b)$. The volumetric momentum transfer rate based on Syamlal's model increases with the averaging size in comparison to that obtained from DEM, which means the correction factor needs to reduce for larger averaging size. This finding simply shows that the growing size of averaging control volume diminishes the effect of big particle such that the correction factor asymptotically reaches to a certain value.

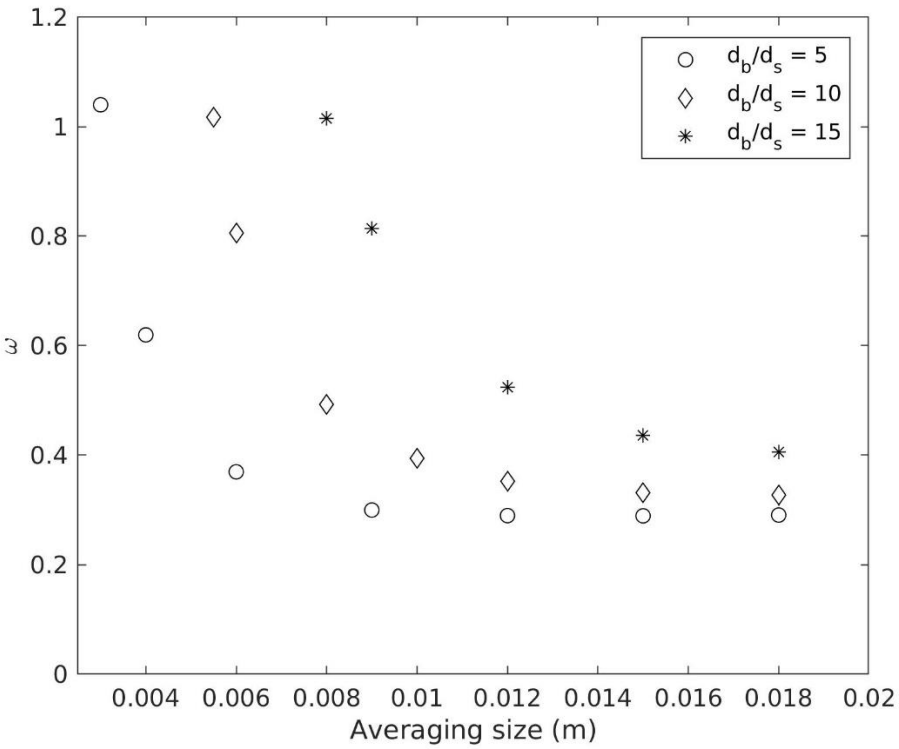

Fig. 6. Correction factor as a function of averaging size for various size ratios.

3.4. Inhomogeneity effects

In the above-mentioned results, we discussed the cases with the width of the stream of small particles greater than the side length of the averaging control volume. Hence, the small particles were homogeneously entering the averaging control volume with a full soaking of the big particle. However, in real gas-solid systems, clusters with various length scales and volume fractions exist which can interact with the larger particles. Therefore, it is crucial to study the effect of inhomogeneity of small particles within the control volume. For this purpose, as sketched in Fig. 7, the width of the stream of small particles is taken smaller than the diameter of big particle, and so the side length of control volume.

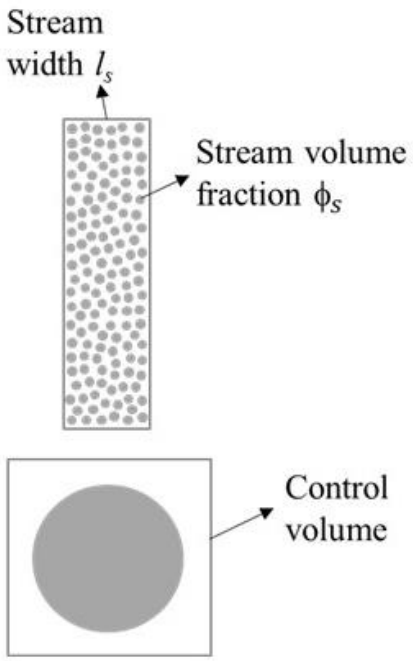

Fig. 7. Schematic of two particle phases for inhomogeneous condition simulations.

For the case of big particle diameter as $15d_s$, various simulation cases are considered for which the stream width l_s was fixed at $12d_s$ with different volume fractions of small particles ϕ_s within the stream. Note that the flow condition, the position of the big particle and the stream height remains the same as in earlier mentioned simulations. In order to study the

interphase momentum transfer rate from the Syamlal's equation, the control volume size was chosen as $20d_s$. The volumetric momentum transfer rate calculated from the DEM (Eq. 11) and the Syamlal's formula are shown in Fig. 8 for different values of the stream volume fractions.

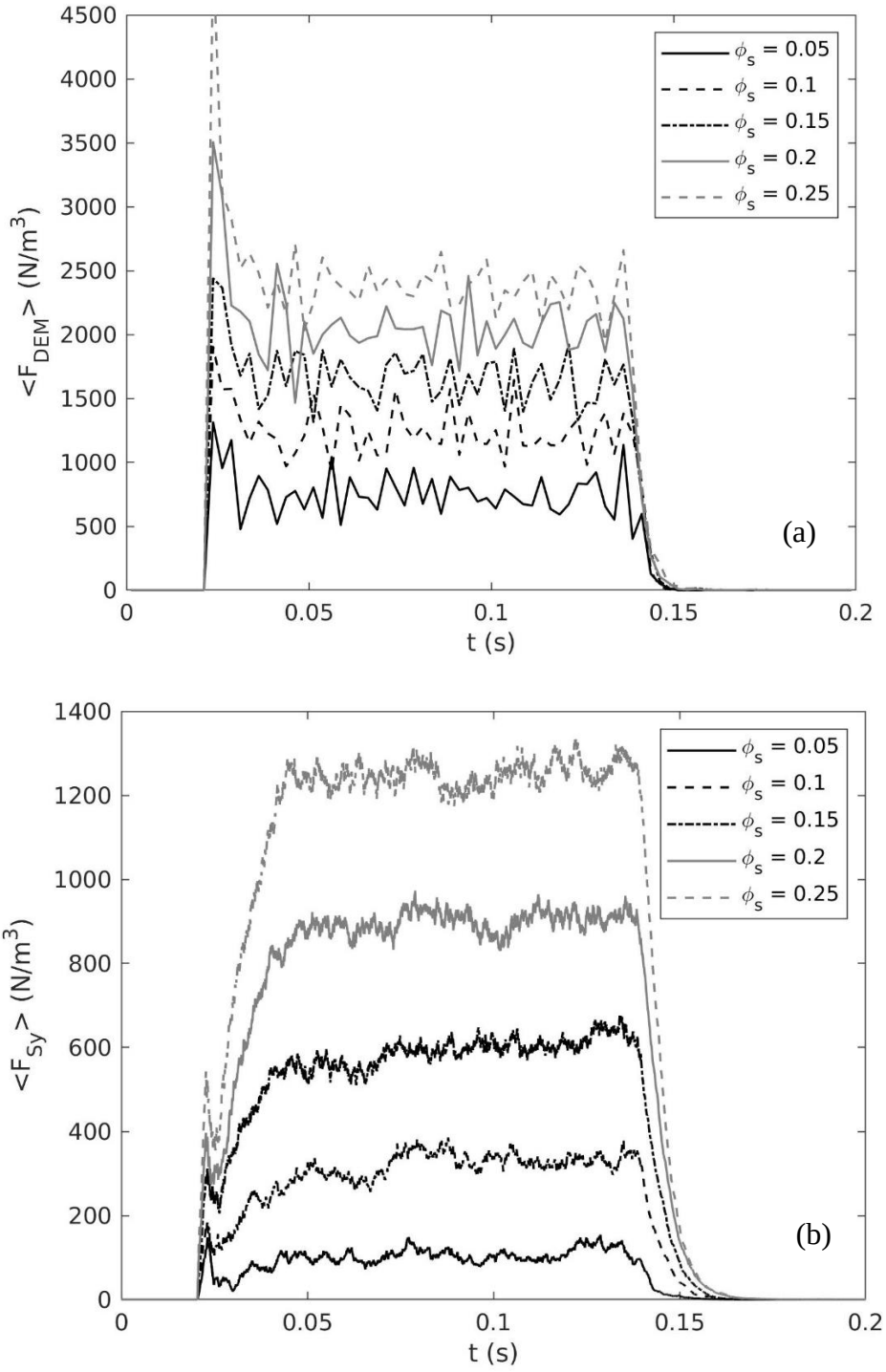

Fig. 8. The volumetric momentum transfer rate for various volume fractions of the stream obtained from (a) DEM and (b) Syamlal formula.

It can be observed from Fig. 8a and 8b that the momentum transfer rate within the steady period increases with the volume fraction of the stream for both the DEM and the Syamlal's formula, though the DEM shows higher magnitudes than the Syamlal's equation. In such cases, the momentum transfer rate due to the Syamlal's formula is underestimated. This is presumably a result of the inhomogeneity in the distribution of the volume fraction of small particles within the control volume. Figure 9 shows that the averaged volume fraction of small particles in the control volume reduces in comparison to the stream volume fraction.

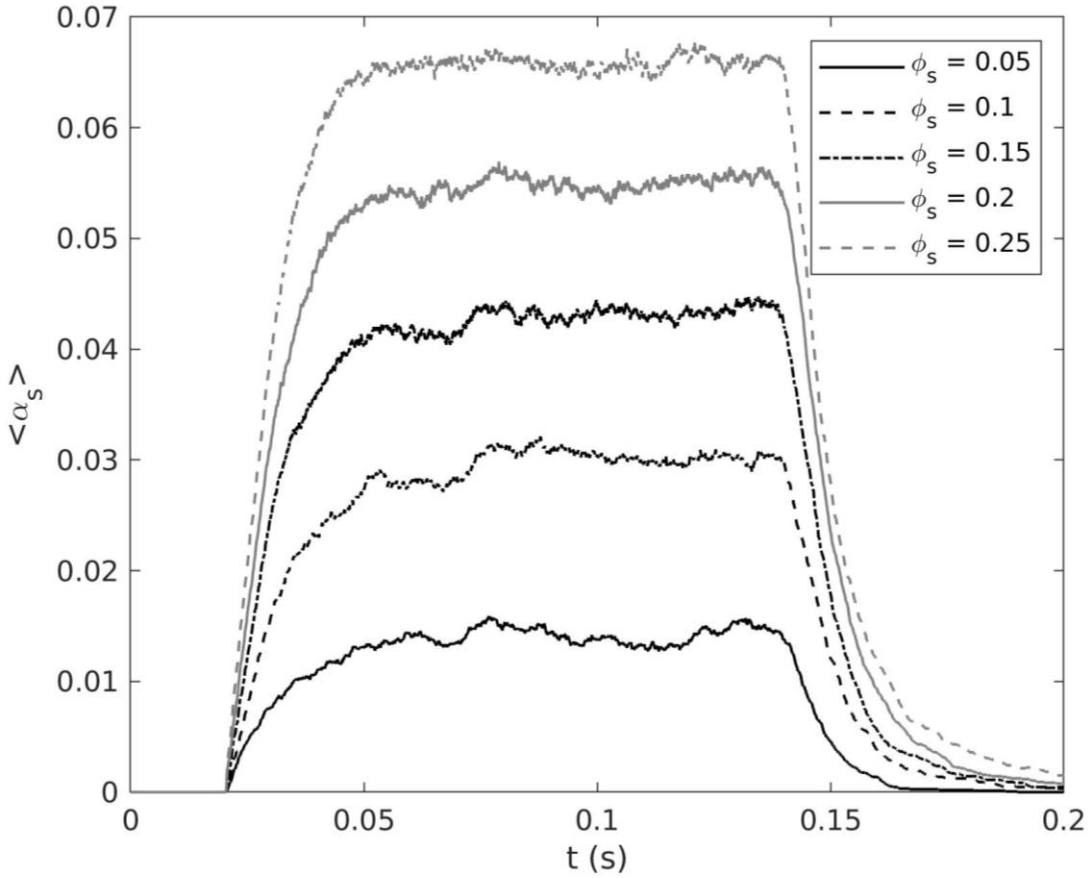

Fig. 9. Time variation of the averaged volume fraction of the small particles in the control volume for different stream volume fractions.

Note that the width of the stream is selected relative to the edge length of the control volume, which is supposed to represent coarse grids in Eulerian simulations. Thus the ratio of the stream width to the control volume edge length is kept below unity to characterize the presence of inhomogeneity in the control volume. The homogeneity of granular phases within

the control volume is a main assumption in the derivation of Syamlal's formula. Thus we need a fine grid in Eulerian simulations to capture the momentum transfer rate correctly. Syamlal's model does not perform well when we increase the size of the averaging region, thus the magnitude of the momentum transfer rate is overestimated and needs to be lowered using a correction factor on the basis of the DEM results. Moreover, the discrepancy between the results of the DEM and the Syamlal's formula can be originated from inhomogeneity, which could lower the mean values of volume fraction fed into the Syamlal's formula. As noted from Fig. 9, the volume fraction in the control volume fluctuates around a constant value during the steady period of the encounter.

Figure 10 depicts how the correction factor calculated from Eq. 12 varies with $\langle \alpha_s \rangle$, an indication factor for the inhomogeneity level of the stream. It can be clearly seen that for smaller $\langle \alpha_s \rangle$ values (larger inhomogeneity) the correction factor is higher whereas it decays as $\langle \alpha_s \rangle$ grows. It is evident that the correction factor has close-to-linear behavior in the higher range of $\langle \alpha_s \rangle$, but it rapidly decays with $\langle \alpha_s \rangle$ in the lower range.

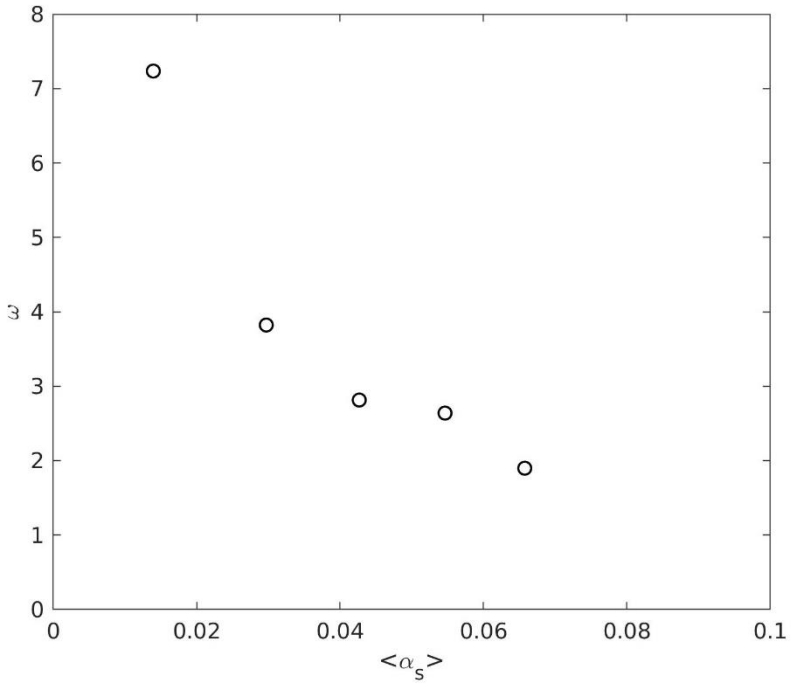

Fig. 10. Variation of correction factor versus averaged volume fraction of small particles in the control volume.

It is worth mentioning that in this section, only the inhomogeneity effects are considered that are due to the difference in the volume fractions of small particles. In general, the prediction of interphase momentum transfer rate with Syamlal's formula depends on variables such as phases volume fractions, size ratio of phases, slip velocity, material properties, density difference and control volume size. Further studies will be performed in future to find suitable correction factor for Syamlal's equation taking into account all those variables.

4. Conclusions

For gas–solid multiphase flows consisting large size ratios, such as in biomass fired fluidized beds, proper modeling for solid-solid momentum transfer rate is required in addition to the gas-solid drag forces for a reasonable representation of the hydrodynamics. In this work, a stream of small particles passing over a single big particle is simulated using DEM in which the size ratio is around 10. Spatial averaging is performed for different averaging regions and the correction factor is obtained for the Syamlal's continuum formula and its dependence on the averaging size is presented.

The correction factor is determined for different size ratios in addition to the size of averaging region. Moreover, the results of current study indicate that the transient encounter results in higher correction factors than those in the steady conditions. Interestingly, the trend of correction factor is such that it remains below 1 as the averaging size increases for all size ratios, though they approach to a unique value for large averaging sizes. In other words, the formula works the best if the size of averaging control volume is close to the size of big particle. If the averaging size is bigger than the big particle size, the averaging size is suggested to be at least twice bigger than the size of big particle in order to apply the same correction factor. In any averaging size, larger size ratio leads to a greater correction factor.

In addition, the effect of the stream volume fraction is studied on the momentum transfer rate when the stream is narrower than the side length of the control volume leading to the creation of an inhomogeneous condition inside the control volume. The results reveal that the momentum transfer rate using the Syamlal's formula is underestimated compared to the predictions of the DEM under imposing of inhomogeneous condition. Thus, there is a need for formulating a correction to Syamlal's formula which takes into account the local inhomogeneity caused by particle phases distributions based on size ratio, material properties, density differences, volume fractions and slip velocity.

In the present study, the variation of slip velocity is not addressed with the momentum transfer rate and the volume fraction of the big particle phase. The future studies will be devoted to develop and implement more comprehensive sub-grid model applicable to coarse grid Eulerian simulations.

Acknowledgements

The authors would like to acknowledge the financial support for this research from the Academy of Finland under grant No. 311138.

References

[1] N. Koukouzas, J. Hämäläinen, D. Papanikolaou, A. Tourunen, T. Jäntti, Mineralogical and elemental composition of fly ash from pilot scale fluidised bed combustion of lignite, bituminous coal, wood chips and their blends, Fuel. 86 (2007) 2186–2193.

[2] T.B. Anderson, R. Jackson, A fluid mechanical description of fluidized beds, Ind. Eng. Chem. Fundam. 6 (1967) 527–539.

[3] P.A. Cundall, O.D.L. Strack, A discrete numerical model for granular assemblies, Geotechnique. 29 (1979) 47–65.

[4] A. Ozel, J. Kolehmainen, S. Radl, S. Sundaresan, Fluid and particle coarsening of drag force for discrete-parcel approach, Chem. Eng. Sci. 155 (2016) 258–267.

[5] Z. Chao, Y. Wang, J.P. Jakobsen, M. Fernandino, H.A. Jakobsen, Investigation of the particle-particle drag in a dense binary fluidized bed, Powder Technol. 224 (2012) 311–322.

[6] M. Syamlal, The particle–particle drag term in a multiparticle model of fluidization, Topical Report, DOE/MC/21353-2373, NTIS/DE87006500, National Technical Information Service, Springfield, VA, 1987.

[7] P. Jalali, T. Hyppänen, Momentum transport between two granular phases of spherical particles with large size ratio: Two-fluid model versus discrete element method, Powder Technol. 273 (2015) 13–18.

[8] P. Jalali, M. Nikku, J. Ritvanen, T. Hyppänen, Flow characteristics of circulating fluidized beds near terminal velocity: Eulerian model of a lab-scale apparatus, Powder Technol. 339 (2018) 569–584.

[9] Y. Igci, A.T. Andrews, S. Sundaresan, S. Pannala, T. O'Brien, Filtered two-fluid models for fluidized gas-particle suspensions, AIChE J. 54 (2008) 1431–1448.

[10] S. Benyahia, On the effect of sub-grid drag closures, Ind. Eng. Chem. Res. 49 (2010) 5122–5131.

[11] J.F. Parmentier, O. Simonin, O. Delsart, A functional subgrid drift velocity model for filtered drag prediction in dense fluidized bed, AIChE J. 58 (2012) 1084–1098.

[12] S. Shah, J. Ritvanen, T. Hyppänen, S. Kallio, Space averaging on a gas-solid drag model for numerical simulations of a CFB riser, Powder Technol. 218 (2012) 131–139.

[13] S. Schneiderbauer, S. Pirker, Filtered and heterogeneity-based subgrid modifications for gas-solid drag and solid stresses in bubbling fluidized beds, AIChE J. 60 (2014) 839–854.

[14] S. Cloete, J.H. Cloete, S. Amini, Hydrodynamic validation study of filtered two fluid models, Chem. Eng. Sci. 182 (2018) 93–107.

[15] W. Holloway, S. Benyahia, C.M. Hrenya, S. Sundaresan, Meso-scale structures of bidisperse mixtures of particles fluidized by a gas, Chem. Eng. Sci. 66 (2011) 4403–4420.

[16] W. Holloway, S. Sundaresan, Filtered models for bidisperse gas-particle flows, Chem. Eng. Sci. 108 (2014) 67–86.

[17] N. Yang, W. Wang, W. Ge, J. Li, CFD simulation of concurrent-up gas-solid flow in circulating fluidized beds with structure-dependent drag coefficient, Chem. Eng. J. 96 (2003) 71–80.

[18] G.J. Heynderickx, A.K. Das, J. De Wilde, G.B. Marin, Effect of clustering on gas−solid drag in dilute two-phase flow, Ind. Eng. Chem. Res. 43 (2004) 4635–4646.

[19] W. Wang, J. Li, Simulation of gas–solid two-phase flow by a multi-scale CFD approach—Extension of the EMMS model to the sub-grid level, Chem. Eng. Sci. 62 (2007) 208–231.

[20] C.C. Milioli, F.E. Milioli, W. Holloway, K. Agrawal, S. Sundaresan, Filtered two-fluid models of fluidized gas-particle flows: New constitutive relations, AIChE J. 59 (2013) 3265–3275.

[21] Y. Tang, E.A.J.F. Peters, J.A.M. Kuipers, Direct numerical simulations of dynamic gas-solid suspensions, AIChE J. 62 (2016) 1958–1969.

[22] L.-T. Zhu, Y.-X. Liu, Z.-H. Luo, An effective three-marker drag model via sub-grid modeling for turbulent fluidization, Chem. Eng. Sci. 192 (2018) 759–773.

[23] L.-T. Zhu, Y.-X. Liu, J.-X. Tang, Z.-H. Luo, A material-property-dependent sub-grid drag model for coarse-grained simulation of 3D large-scale CFB risers, Chem. Eng. Sci. 204 (2019) 228–245.

[24] C. Kloss, C. Goniva, A. Hager, S. Amberger, S. Pirker, Models, algorithms and validation for opensource DEM and CFD-DEM, Prog. Comput. Fluid Dyn. 12 (2012) 140–152.

[25] Y. Tsuji, T. Tanaka, T. Ishida, Lagrangian numerical simulation of plug flow of cohesionless particles in a horizontal pipe, Powder Technol. 71 (1992) 239–250.

[26] A. Di Renzo, F.P. Di Maio, Comparison of contact-force models for the simulation of collisions in DEM-based granular flow codes, Chem. Eng. Sci. 59 (2004) 525–541.

[27] P. Jalali, M. Nikku, T. Hyppänen, Particle-cloud drag force in dilute particle systems: Discrete element methods versus Eulerian simulations, Ind. Eng. Chem. Res. 52 (2013) 4342–4350.

[28] A.T. Andrews IV, P.N. Loezos, S. Sundaresan, Coarse-grid simulation of gas-particle flows in vertical risers, Ind. Eng. Chem. Res. 44 (2005) 6022–6037.

[29] J. Wang, M.A. van der Hoef, J.A.M. Kuipers, Why the two-fluid model fails to predict the bed expansion characteristics of Geldart A particles in gas-fluidized beds: A tentative answer, Chem. Eng. Sci. 64 (2009) 622–625.